Drag, deformation, and drift volume associated with a drop rising in a density stratified fluid

Vaseem A. Shaik and Arezoo M. Ardekani*
School of Mechanical Engineering, Purdue University, West Lafayette, Indiana 47907, USA

(Received 7 March 2019; published 29 January 2020)

We consider a drop of constant density and uniform interfacial tension rising in a linearly density stratified fluid. In the limits of weak inertia and stratification effects, we calculate the drag acting on the drop, the flow fields inside and outside the drop, the drop deformation, and the drift volume induced by the drop using the method of matched asymptotic expansions. Stratification or inertia increase the drag, and this enhanced drag acting on a drop is equal to $(\frac{3\lambda+2}{3(\lambda+1)})^2$ times the enhanced drag acting on a rigid sphere, where λ is the viscosity ratio. This relation between the enhanced drags of a drop and a rigid sphere holds even in the presence of both of these effects (stratification and inertia). On the other hand, stratification does not result in any deformation of the drop up to the first order of approximation. At zero inertia and small advective transport rate of density, the drift volume induced by the drop rising in a stratified fluid is finite (but large compared to the drop's volume), unlike the drift volume in a homogeneous fluid, which is infinite.

DOI: 10.1103/PhysRevFluids.5.013604

I. INTRODUCTION

In lakes, ponds, or oceans, the variation of temperature or salt concentration with height causes density stratification. Drops in stratified fluids are encountered when one uses bubble plumes for destratification to get rid of the harmful effects associated with the stratification [1] or during an oil spill as oil drops rise through stratified water in the ocean [2]. It is then necessary to find the forces acting on a drop rising in a stratified fluid to estimate the efficiency of the destratification process or to understand the consequences of an oil spill [3].

There was a tremendous effort to understand the settling motion of spheres in a stratified fluid for different values of Re, Fr, and Pr, which denote the Reynolds, Froude, and Prandtl numbers, respectively [3–13]. These works used two types of stratification—linearly stratified fluid or two homogeneous miscible fluids of different densities separated by a density stratified interface of finite or zero thickness (call this step stratification). All these works reported a drag enhancement due to stratification, the physics behind this drag enhancement being dependent on the type of stratification, Re, and Fr.

For a sphere settling through a step stratification at $1.5 < \mathrm{Re} < 15$, it was found that its velocity changes nonmonotonically from its terminal velocity in the upper fluid to its terminal velocity in the lower fluid displaying a minimum somewhere in the interface due to the stratification enhanced drag [5]. A similar nonmonotonic variation of the settling velocity with time was also found for a sphere crossing an interface separating two homogeneous fluids (with zero interface thickness) even at zero Re [7,8]. Again considering the settling through step stratification at $20 < \mathrm{Re} < 450$, it was found that the sphere decelerates so much due to enhanced drag that it levitates (comes to rest in a fluid that is lighter than it) and reverses its direction of motion for some time before continuing to fall down [6]. In these works, the sphere leaving the upper homogeneous fluid (by entering the stratified

*ardekani@purdue.edu

interface or lower homogeneous fluid) drags this low-density fluid with it, and the buoyancy of this low-density fluid manifests as an enhanced drag on the sphere. As long as the low-density fluid is attached to the sphere, it decelerates achieving a minimum velocity, at which point the entire low-density fluid is detached from the sphere due to which it begins to accelerate. This leads to the nonmonotonic variation of velocity with time.

When a sphere is settling through a linearly stratified fluid at moderate Re ($10 < \mathrm{Re} < 1000$), it was observed that a standing vortex, which typically occurs in homogeneous fluids, is suppressed by stratification, in turn giving rise to a strong vertical jet behind the sphere [9–11]. A mechanism for the appearance of this jet is given as follows. As the sphere settles, it drags a low-density fluid, which initially is located near the front of the sphere in the density boundary layer. Due to the buoyancy, this low-density fluid rises to the back of the sphere in an attempt to return to its original position, in turn generating a vertical jet. This jet is similar to the caudal fluid dragged from the upper homogeneous layer when a sphere is settling in a step stratification. The buoyancy of the low-density fluid in the jet and the generated internal waves as low-density fluid returns to its initial density level are responsible for the increased drag due to stratification [12].

The physics associated with a particle settling in a linearly stratified fluid at moderate Re is interesting yet quite complex to understand, as in this case after the particle reaches its peak velocity, other than monotonic deceleration, the particle can levitate momentarily, reverse its direction of motion, and even oscillate with a frequency proportional to the Brunt-Väisälä frequency [12]. The wake structure behind such a settling particle is also complicated and can be one of the seven types depending on Re and Fr [14]. On the other hand, settling at low Re is well understood. In this case, the buoyancy of a light fluid immediately adjacent to the sphere manifests as the enhanced drag, which was shown to be proportional to $\mathrm{Ri}^{0.51}$, where Ri is the viscous Richardson number [15].

Most of the previous works attributed the stratification enhanced drag to the buoyancy of the dragged lighter fluid. In an attempt to identify the origin of this stratification enhanced drag, a recent work [16] divided the contributions of the stratification to the drag into two parts—the first one coming from the buoyancy of the lighter fluid and the second one arising from the baroclinic torque induced modifications in the vorticity field around the settling particle. For most values of Re, Fr, and Pr, the force due to the change in vorticity dominates and is responsible for the observed stratification enhanced drag.

A few theoretical works were also carried out to derive the stratification enhanced drag acting on a particle settling in a linearly stratified fluid [17–19]. Due to the coupling between the equations governing the fluid flow and density transport, such a calculation was only done for weak stratifications, in turn enabling one to take perturbations in terms of a small stratification parameter. It was shown that such perturbation is singular, similar to the perturbation in Re [20], as the matching zone where the viscous forces balance the buoyancy forces occurs far away from the particle. The exact location of the matching zone depends on whether advection of density transport dominates the diffusion or vice versa. Neglecting inertia, Zvirin and Chadwick [17] calculated this stratification enhanced drag assuming the advection is more important, while work of [18] is valid if diffusion is more important. It was recently shown in Ref. [19] that Zvirin and Chadwick's calculation holds not only in the limits of dominant advection or dominant diffusion, but also uniformly between these two limits. The main focus of Ref. [19] was to estimate the inertial effects on the stratification enhanced drag for a settling rigid particle. We use a similar perturbation scheme to find the influence of inertia on the stratification enhanced drag acting on a rising drop. We extend the scope of the work by evaluating the drop deformation, flow field and the drift volume induced by the drop as well.

There are few numerical works that analyzed the settling or rising dynamics of a drop in a stratified fluid. In this case, either the stratification or the presence of surfactants can cause the spatial inhomogeneities in the interfacial tension that complicate the rising dynamics [21,22]. Analyzing the settling motion of a drop in a step stratification, it was found that the slip boundary condition on the drop causes it to entrain less amount of low-density fluid than that of a rigid sphere, which manifests as a smaller stratification enhanced drag [21]. Similar to a settling particle, a drop rising in a linearly stratified fluid at moderate Re can levitate, reverse its direction of motion, and even oscillate about a certain fluid density level [23]. In a linearly stratified fluid, two drops rising in tandem or in

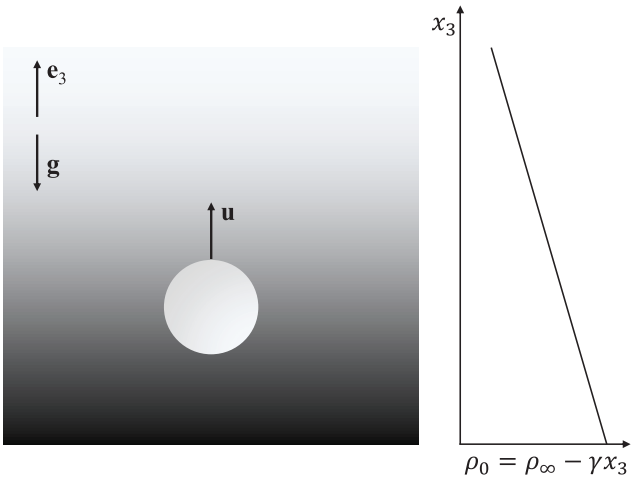

FIG. 1. A schematic showing a drop of constant density and uniform interfacial tension rising through a stratified fluid whose ambient density $\rho_0 = \rho_\infty - \gamma x_3$ decreases with the height. Also shown is a unit vector $\mathbf{e}_3$ pointing vertically upward and a gravity vector $\mathbf{g} = -g\mathbf{e}_3$.

a side-by-side configuration were found to retain their configuration during interaction [24]. This observation for drops in tandem motion in a stratified fluid holds for stronger stratifications and is in contrast to their motion in a homogeneous fluid. After the drops approach their neutrally buoyant density level, they oscillate, and eventually the trailing drop rotates around the leading one, forming a side-by-side configuration. For a swarm of drops rising in a linearly stratified fluid, it was reported that the stratification hinders the vertical rise velocity of the swarm but increases the probability of cluster formation [25].

A drop rising in a homogeneous or stratified fluid drags a certain volume of fluid with it, the so called drift volume. An estimate of drift volume induced by a rising drop would answer if the drop mixes its surrounding environment. It was Darwin [26] who introduced the drift volume, and he found that the drift volume induced by a translating sphere in an inviscid fluid is equal to the added mass divided by the fluid density. In a viscous fluid, at $\mathrm{Re} = 0$, Eames *et al.* calculated the drift volume induced by a rising drop and found that a slow $1/r$ velocity decay causes the drift volume to become infinite [27]. They also evaluated the drift volume induced by a drop translating normal to a wall, and they found that a faster $1/r^3$ velocity decay makes the drift volume finite but much large compared to the drop's volume. Here r is the distance measured from the center of the drop. At finite Re, the ever increasing extent of wake behind a towed particle and a slow $1/r$ decay of velocity in the wake produces an infinite drift volume [28]. Such infinite drift volume induced by towing particles at zero or finite Re prompted the drift based explanations in support of biogenic mixing contributions to oceanic circulation [29,30]. But effects such as density stratification [12,31,32], background turbulence [33], and the force-free nature of swimming organisms [34] reduce the drift volume and make it finite.

Despite several studies on the subject, a theoretical investigation of drop transport in a stratified fluid and the induced drift volume is missing, which is the focus of the present work. This paper is organized as follows. We present the dimensionless governing equations and boundary conditions in Sec. II. We then derive the drag, first-order flow fields, drop deformation, and the induced drift volume in Secs. III, IV, V, and VI, respectively. We provide some concluding remarks in Sec. VII.

II. PROBLEM FORMULATION

In this section, we present the dimensionless governing equations and boundary conditions for the fluid flow and density disturbance when a drop is rising in a stratified fluid (see Fig. 1 for a

schematic). We work in a frame moving with the drop. In this frame, the drop is stationary and the fluid velocity $\mathbf{w}$ far away from the drop approaches the negative of the drop velocity $\mathbf{u}$, i.e., $\mathbf{w} \sim -\mathbf{u}$ as $r = |\mathbf{r}| \to \infty$. In this far-field region, the fluid density ρ is equal to the ambient density ρ_0 that varies linearly with the vertical position x_3, i.e., $\rho \sim \rho_0 = \rho_\infty - \gamma x_3$ as $r \to \infty$. Here, $\mathbf{r}$ and $\mathbf{x}$ are the position vectors with respect to the drop center and a fixed point in the laboratory frame, so $\mathbf{x} = \mathbf{r} + \mathbf{x}_d$, where $\mathbf{x}_d$ gives the drop's position in the laboratory frame. Also ρ_∞ is the reference density while $\gamma > 0$ is the density gradient. The pressure p in the far field is equal to p_0, which is governed by $-\nabla p_0 + \rho_0 \mathbf{g} = \mathbf{0}$, where $\mathbf{g} = -g\,\mathbf{e}_3$ is a gravity vector whose magnitude is equal to the acceleration due to gravity g, and $\mathbf{e}_3$ is a unit vector pointing vertically upward.

We define the disturbance velocity, pressure, and density fields outside the drop as $\mathbf{w}' = \mathbf{w} + \mathbf{u}$, $p' = p - p_0$, $\rho' = \rho - \rho_0$. Here we use the Boussinesq approximation. The disturbance pressure, velocity, and density outside the drop are governed by the continuity, Navier-Stokes, and the advection-diffusion equations,

$$\nabla \cdot \mathbf{w}' = \mathbf{0}, \tag{1}$$

$$\rho_\infty \left[\frac{\partial \mathbf{w}'}{\partial t} + (\mathbf{w}' \cdot \nabla)\mathbf{w}' - (\mathbf{u} \cdot \nabla)\mathbf{w}' \right] = -\nabla p' + \rho_\infty \nu \nabla^2 \mathbf{w}' + \rho' \mathbf{g}, \tag{2}$$

$$\frac{\partial \rho'}{\partial t} + \mathbf{w}' \cdot \nabla \rho' - \mathbf{u} \cdot \nabla \rho' - \gamma(\mathbf{w}' \cdot \mathbf{e}_3) = \kappa \nabla^2 \rho'. \tag{3}$$

Here ν is the kinematic viscosity of the fluid outside the drop and κ is the diffusivity. In general, the variations in density are caused by the variations in temperature or salt concentration. For small changes in temperature or salt concentrations, these changes are linearly proportional to the changes in density, and in this case we can directly write an advection-diffusion equation for density, with κ being the diffusion coefficient of the associated transport phenomenon (thermal or salt transport).

We assume the density of the fluid inside the drop ρ_d to be constant. Writing the pressure inside the drop p_d as $p_d = p_d' - \rho_d g x_3$, we find that the fluid flow $\mathbf{w}_d$ and the pressure field inside the drop are governed by

$$\nabla \cdot \mathbf{w}_d = \mathbf{0}, \tag{4}$$

$$\rho_d \left[\frac{\partial \mathbf{w}_d}{\partial t} + (\mathbf{w}_d \cdot \nabla)\mathbf{w}_d \right] = -\nabla p_d' + \rho_d \nu_d \nabla^2 \mathbf{w}_d - \rho_d \frac{d\mathbf{u}}{dt}, \tag{5}$$

where ν_d is the kinematic viscosity of the fluid inside the drop.

We use the undeformed drop radius a, timescale t_c, and the drop speed in a homogeneous fluid of reference density u_c to nondimensionalize the length, time, and velocity. We nondimensionalize the density by γa while the pressure or stress field outside (resp. inside) the drop is nondimensionalized by $\rho_\infty \nu u_c/a$ (resp. $\rho_d \nu_d u_c/a$). We find that the dimensionless governing equations and the boundary conditions are characterised by six dimensionless parameters: the Reynolds number Re, which is the ratio of inertia forces to the viscous forces, the Péclet number Pe, which is the ratio of the advective transport rate of density to its diffusive transport rate, the viscous Richardson number Ri, which is the ratio of buoyancy forces to the viscous forces, the Strouhal number St, which is the ratio of advective timescale to the characteristic time scale t_c, the dynamic viscosity ratio λ, and the kinematic viscosity ratio χ. Their expressions are given as

$$\mathrm{Re} = \frac{a u_c}{\nu}, \quad \mathrm{Pe} = \frac{a u_c}{\kappa}, \quad \mathrm{Ri} = \frac{\gamma a^3 g}{\rho_\infty \nu u_c}, \quad \mathrm{St} = \frac{a}{u_c t_c}, \quad \lambda = \frac{\rho_d \nu_d}{\rho_\infty \nu}, \quad \chi = \frac{\nu_d}{\nu}. \tag{6}$$

We carry out a quasisteady analysis in which we neglect the unsteady terms proportional to ReSt or PeSt or ReSt/χ. This analysis is valid for $\mathrm{Re} \ll 1$, $\mathrm{Ri} \ll 1$, and $\chi \geqslant 1$ as in this case we can estimate the timescale of velocity variations t_c and show that $\mathrm{St} \sim \mathrm{Ri}$ [19], which makes the unsteady terms smaller than the rest of the terms in any governing equation. We rewrite Re, Pe, and Ri in terms of $\epsilon = a/l_s$, l_s/l_o, and Pr [18]. Here $l_s = (\nu\kappa/N^2)^{1/4}$ is the stratification length scale [35],

the distance from the drop at which the buoyancy forces become as important as the viscous forces when Pe $\ll 1$, where $N = \sqrt{g\gamma/\rho_\infty}$ is the Brunt-Väisälä frequency, the typical frequency at which a displaced fluid parcel in a stratified fluid oscillates. Also $l_o = a/\mathrm{Re}$ is the Oseen length scale, the distance from the drop at which the inertia forces balance the viscous forces, and $\mathrm{Pr} = \nu/\kappa$ is the Prandtl number. Hence, the dimensionless governing equations for the disturbance flow and the disturbance density outside the drop after rescaling the density as $\tilde{\rho} = \frac{\rho'}{\mathrm{Pe}} = \frac{\rho'}{\epsilon \frac{l_s}{l_o} \mathrm{Pr}}$ are

$$\nabla \cdot \mathbf{w}' = \mathbf{0}, \tag{7}$$

$$\epsilon \frac{l_s}{l_o}[(\mathbf{w}' \cdot \nabla)\mathbf{w}' - (\mathbf{u} \cdot \nabla)\mathbf{w}'] = -\nabla p' + \nabla^2 \mathbf{w}' - \epsilon^4 \tilde{\rho}\, \mathbf{e}_3, \tag{8}$$

$$-\mathbf{w}' \cdot \mathbf{e}_3 + \epsilon \frac{l_s}{l_o} \mathrm{Pr}[\mathbf{w}' \cdot \nabla \tilde{\rho} - \mathbf{u} \cdot \nabla \tilde{\rho}] = \nabla^2 \tilde{\rho}. \tag{9}$$

Similarly, the flow field inside the drop is governed by

$$\nabla \cdot \mathbf{w}_d = \mathbf{0}, \tag{10}$$

$$\frac{\epsilon}{\chi} \frac{l_s}{l_o}(\mathbf{w}_d \cdot \nabla)\mathbf{w}_d = -\nabla p'_d + \nabla^2 \mathbf{w}_d. \tag{11}$$

Far away from the drop, the disturbance velocity and the disturbance density decay to zero,

$$\mathbf{w}' = \mathbf{0} \quad \text{and} \quad \tilde{\rho} = 0 \text{ as } r \to \infty. \tag{12}$$

At the drop surface, the flow field normal to the drop must be zero,

$$\mathbf{n} \cdot \mathbf{w}_d = \mathbf{n} \cdot (\mathbf{w}' - \mathbf{u}) = 0 \text{ on the drop.} \tag{13}$$

The flow field tangential to the drop must be continuous across the drop surface,

$$(\mathbf{I} - \mathbf{nn}) \cdot \mathbf{w}_d = (\mathbf{I} - \mathbf{nn}) \cdot (\mathbf{w}' - \mathbf{u}) \text{ on the drop.} \tag{14}$$

The shear stress must be continuous across the drop surface,

$$\mathbf{n} \cdot (\mathbf{T}' - \lambda \mathbf{T}_d) \cdot (\mathbf{I} - \mathbf{nn}) = \mathbf{0} \text{ on the drop.} \tag{15}$$

Here $\mathbf{n}$ is the vector normal to the drop pointing into the suspending fluid, $\mathbf{I}$ is the identity tensor, $\mathbf{T}'$ (resp. $\mathbf{T}_d$) is the stress tensor associated with the disturbance flow outside the drop $\mathbf{w}'$ (resp. the flow inside the drop $\mathbf{w}_d$), which using the Newtonian constitutive relation can be written as $\mathbf{T}' = -p'\mathbf{I} + [\nabla \mathbf{w}' + (\nabla \mathbf{w}')^\dagger]$, $\dagger$ represents the transpose. We impose the no flux condition on the drop surface for the density field, which is equivalent to ensuring that the drop surface is adiabatic (resp. impermeable) for the stratification caused by thermal transport (resp. salt transport),

$$\frac{\partial \tilde{\rho}}{\partial r} = \frac{\cos\theta}{\mathrm{Pe}} = \frac{\cos\theta}{\epsilon \frac{l_s}{l_o} \mathrm{Pr}} \text{ on the drop,} \tag{16}$$

where $\cos\theta = \frac{\mathbf{r} \cdot \mathbf{e}_3}{r} = \frac{r_3}{r}$.

We solve Eqs. (7)–(16) to find the drag and deformation of a drop along with the flow field in the limit

$$\epsilon \ll 1, \quad \frac{l_s}{l_o} \ll \epsilon^{-1}, \quad \chi \geqslant 1, \quad \mathrm{Pr}, \quad \lambda \text{ arbitrary but fixed.} \tag{17}$$

III. DRAG

We expand the field variables inside the drop and in the inner zone close to the drop as follows:

$$\{\mathbf{w}', p', \tilde{\rho}, \mathbf{w}_d, p'_d\} = \{\mathbf{w}'_0, p'_0, \tilde{\rho}_0, \mathbf{w}_{0,d}, p'_{0,d}\} + \epsilon\{\mathbf{w}'_1, p'_1, \tilde{\rho}_1, \mathbf{w}_{1,d}, p'_{1,d}\} + o(\epsilon). \tag{18}$$

We find that the leading-order flow variables ($\mathbf{w'}_0$, p'_0, $\mathbf{w}_{0,d}$, $p'_{0,d}$) satisfy the Stokes equations for a homogeneous fluid whose solution is well known [36]. The leading-order drag experienced by the drop is $\mathbf{F}_0 = -2\pi\mathcal{R}\mathbf{u}$, where $\mathcal{R} = (2+3\lambda)/(1+\lambda)$ and it varies from 2 (for a bubble) to 3 (for a rigid sphere). It was already reported that the drop does not deform due to this leading-order flow (see Sec. V for more details) [37,38]. So we can consider a spherical drop to solve the first-order problem.

We now use the leading-order inner flow $\mathbf{w'}_0$ to estimate the order of magnitude of various terms in the Navier-Stokes and density transport equations in the matching zone that occurs at $r \gg 1$. As $\mathbf{w'}_0 \sim 1/r$ for $r \gg 1$, we see that $\mathbf{w'} \cdot \nabla \mathbf{w'} \sim 1/r^3$ while $\mathbf{u} \cdot \nabla \mathbf{w'} \sim 1/r^2$ for $r \gg 1$. Hence we neglect $\mathbf{w'} \cdot \nabla \mathbf{w'}$ as compared to $\mathbf{u} \cdot \nabla \mathbf{w'}$ for $r \gg 1$. Similarly, we notice that $\mathbf{w'} \cdot \nabla \tilde{\rho} \sim \tilde{\rho}/r^2$ and $\mathbf{u} \cdot \nabla \tilde{\rho} \sim \tilde{\rho}/r$ for $r \gg 1$ due to which we neglect $\mathbf{w'} \cdot \nabla \tilde{\rho}$ in comparison to $\mathbf{u} \cdot \nabla \tilde{\rho}$ in the matching zone. So the equations governing the leading-order flow disturbance and density disturbance in the matching or outer zone at $r \gg 1$ are

$$\nabla \cdot \mathbf{w'} = \mathbf{0}, \tag{19}$$

$$-\epsilon \frac{l_s}{l_o}(\mathbf{u} \cdot \nabla \mathbf{w'}) = -\nabla p' + \nabla^2 \mathbf{w'} - \epsilon^4 \tilde{\rho}\, \mathbf{e}_3 + 2\pi\mathcal{R}\mathbf{u}\delta(\mathbf{r}), \tag{20}$$

$$-\mathbf{w'} \cdot \mathbf{e}_3 - \epsilon \frac{l_s}{l_o} \mathrm{Pr}\,(\mathbf{u} \cdot \nabla)\tilde{\rho} = \nabla^2 \tilde{\rho}. \tag{21}$$

In the far field, we represent the drop by a point force equal to the negative of drag acting on the drop [39,40], which justifies the source term $-\mathbf{F}_0\,\delta(\mathbf{r}) = 2\pi\mathcal{R}\mathbf{u}\,\delta(\mathbf{r})$ appearing in Eq. (20). The no-flux boundary condition for density on the drop surface precludes such source terms in the density transport equation.

As Eqs. (19)–(21) are linear, we solve them by taking the Fourier transform where the Fourier and inverse Fourier transforms are defined as

$$\hat{\mathbf{w}}'(\mathbf{k}) = \int d\mathbf{r}\, \mathbf{w}'(\mathbf{r}) e^{-i\mathbf{k}\cdot\mathbf{r}} \quad \text{and} \quad \mathbf{w}'(\mathbf{r}) = \frac{1}{8\pi^3} \int d\mathbf{k}\, \hat{\mathbf{w}}'(\mathbf{k}) e^{i\mathbf{k}\cdot\mathbf{r}}, \tag{22}$$

where $i = \sqrt{-1}$. In the Fourier space, the disturbance flow in the outer zone is given by

$$\hat{\mathbf{w}}' = 2\pi\mathcal{R}[\mathscr{A} - \epsilon^4\mathscr{B} + \epsilon^4\mathscr{D}]^{-1}\mathscr{E}\mathbf{u}, \quad \text{where} \tag{23}$$

$$\mathscr{A} = \left[k^2 - i\epsilon\frac{l_s}{l_o}(\mathbf{u}\cdot\mathbf{k})\right]\mathbf{I}, \quad \mathscr{B} = \frac{k_3}{k^2\left[k^2 - i\epsilon\frac{l_s}{l_o}\mathrm{Pr}\,(\mathbf{u}\cdot\mathbf{k})\right]}\mathbf{k}\mathbf{e}_3,$$

$$\mathscr{D} = \frac{\mathbf{e}_3\mathbf{e}_3}{\left[k^2 - i\epsilon\frac{l_s}{l_o}\mathrm{Pr}\,(\mathbf{u}\cdot\mathbf{k})\right]}, \quad \text{and} \quad \mathscr{E} = \left(\mathbf{I} - \frac{\mathbf{k}\mathbf{k}}{k^2}\right).$$

We represented the second-order tensors as matrices while the vectors are represented as column vectors in Eq. (23). We interpret $\hat{\mathbf{w}}'$ as a generalized function, and for $\epsilon \ll 1$ we perform a Taylor series expansion about $\epsilon = 0$ to obtain

$$\hat{\mathbf{w}}' = \hat{\mathscr{T}}'_0 + \epsilon\hat{\mathscr{T}}'_1 + \cdots + \epsilon^n\hat{\mathscr{T}}'_n, \quad \text{where} \quad \hat{\mathscr{T}}'_n = \lim_{\epsilon\to 0}\frac{1}{n!}\frac{d^n\hat{\mathbf{w}}'}{d\epsilon^n}. \tag{24}$$

We find that $\hat{\mathscr{T}}'_0$ is the Fourier transform of the Stokeslet flow field $\mathbf{w}_S$ that is governed by

$$\nabla \cdot \mathbf{w}_S = \mathbf{0}, \quad -\nabla p_S + \nabla^2 \mathbf{w}_S + 2\pi\mathcal{R}\mathbf{u}\,\delta(\mathbf{r}) = \mathbf{0}. \tag{25}$$

It can be shown that in the matching zone, the inverse Fourier transform of $\hat{\mathscr{T}}'_0$ matches with the Stokeslet part of the leading-order inner flow $\mathbf{w'}_0$.

We write $\hat{\mathscr{T}}_1'$ as

$$\begin{aligned}\hat{\mathscr{T}}_1' &= \lim_{\epsilon\to 0}\frac{1}{\epsilon}[\hat{\mathbf{w}}'(\mathbf{k}) - \hat{\mathscr{T}}_0'(\mathbf{k})] = \lim_{\epsilon\to 0}\frac{1}{\epsilon}[\hat{\mathbf{w}}'(\mathbf{k}) - \hat{\mathbf{w}}_S(\mathbf{k})]\\ &= \lim_{\epsilon\to 0}\frac{1}{\epsilon^3}\left[\hat{\mathbf{w}}'\left(\frac{\mathbf{k}}{\epsilon}\right) - \hat{\mathbf{w}}_S\left(\frac{\mathbf{k}}{\epsilon}\right)\right] = \delta(\mathbf{k})\int d\mathbf{k}'\left[\hat{\mathbf{w}}'\left(\frac{\mathbf{k}'}{\epsilon}\right) - \hat{\mathbf{w}}_S\left(\frac{\mathbf{k}'}{\epsilon}\right)\right]_{\epsilon=1}\\ &= \delta(\mathbf{k})\int d\mathbf{k}'[\hat{\mathbf{w}}'|_{\epsilon=1}(\mathbf{k}') - \hat{\mathbf{w}}_S(\mathbf{k}')],\end{aligned} \tag{26}$$

where $\hat{\mathbf{w}}_S$ is the Fourier transform of $\mathbf{w}_S$, $\delta(\mathbf{k})$ is the delta function, and we used the properties of generalized functions to evaluate the limit [41,42]. We find that the inverse Fourier transform of $\hat{\mathscr{T}}_1'$ is given by

$$\mathscr{T}_1' = \frac{1}{8\pi^3}\int d\mathbf{k}'[\hat{\mathbf{w}}'|_{\epsilon=1}(\mathbf{k}') - \hat{\mathbf{w}}_S(\mathbf{k}')]. \tag{27}$$

This is a uniform flow, and it should match with the uniform flow part of $\mathbf{w}'_1$ in the matching zone.

We only need the knowledge of the flow field in the outer zone to determine the first-order force acting on the drop. This force is given by [43]

$$\mathbf{F}_1 = 2\pi\mathcal{R}\mathscr{T}_1'. \tag{28}$$

Using $\mathbf{u} = u_3\mathbf{e}_3$ we find that $\mathscr{T}_1' = -M_{33,\text{drop}}u_3\mathbf{e}_3$ and the drag acting on the drop is $\mathbf{F} = F_3\mathbf{e}_3$, where

$$F_3 = -2\pi\mathcal{R}u_3(1+\epsilon\, M_{33,\text{drop}}), \quad M_{33,\text{drop}} = \frac{\mathcal{R}}{3}M_{33,\text{rgsp}}, \quad \text{and} \tag{29}$$

$$M_{33,\text{rgsp}} = -\frac{3}{2\pi}\int_0^\infty dk\int_0^\pi d\theta\,\frac{\sin^3\theta\left\{1-\left[\text{Pr}\left(\frac{l_s}{l_o}\right)^2u_3^2k^2+1\right]\cos^2\theta - i\cos\theta\frac{l_s}{l_o}u_3k^3\right\}}{\left[\text{Pr}\left(\frac{l_s}{l_o}\right)^2u_3^2k^2+1\right]\cos^2\theta + i\frac{l_s}{l_o}u_3k^3(\text{Pr}+1)\cos\theta - k^4 - 1}. \tag{30}$$

The expression for $M_{33,\text{rgsp}}|_{u_3=1}$ is the same as that reported by Mehaddi *et al.* (see Eq. 5.3b in Ref. [19]) for a falling rigid sphere in a stratified fluid except that there is a missing negative sign in their expression. From Eq. (29), we see that the stratification enhanced drag acting on a drop is equal to $(\mathcal{R}/3)^2$ times the enhanced drag on a rigid sphere. As the governing equations and the boundary conditions associated with the leading-order and the first-order flows in the inner zone and inside the drop derived in our work are the same as those reported for a drop moving in a shear flow of a homogeneous fluid (in the limit of zero shear rate), we can use the physical arguments reported in the latter case [37] to find the scaling of stratification enhanced drag with $\mathcal{R}$. This way, we can deduce the form of drag force, Eq. (29), without finding any of the flow fields. According to these arguments, one relates the drag force with the strength of vorticity on the drop surface. It is evident from Eq. (20) that the disturbance flow in the outer zone is proportional to $\mathcal{R}$ and hence the uniform flow $\mathscr{T}_1' \propto \mathcal{R}$. To satisfy this uniform flow boundary condition at infinity, a vorticity of strength proportional to $\mathcal{R}\mathscr{T}_1'$ is induced on the drop surface, which justifies why $\mathbf{F}_1 \propto \mathcal{R}^2$. We plot the stratification enhanced drag acting on a bubble for various l_s/l_o and Pr in Fig. 2.

We can simplify the expression for drag in some limiting cases. For $l_s/l_o \ll \text{Pr}^{-1}$, the buoyancy forces balance the viscous forces in the matching zone, and the density transport is governed by

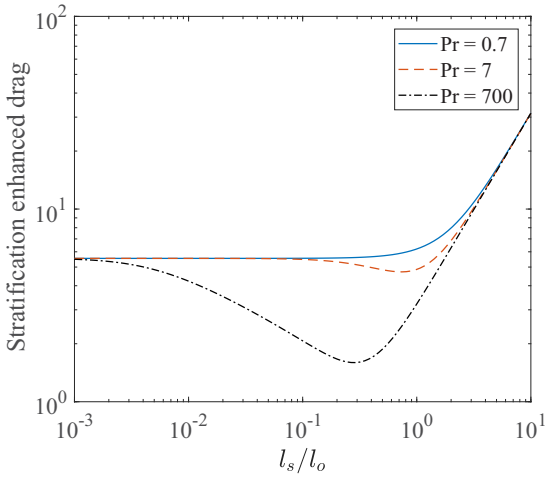

FIG. 2. The variation of the stratification enhanced drag acting on a bubble, $8\pi M_{33,\mathrm{rgsp}}/3$, with l_s/l_o and Pr. The blue solid, red dashed, and black dash-dotted lines denote the data for Pr = 0.7, 7 (temperature stratified water), and 700 (salt stratified water), respectively. This variation of drag acting on a bubble with l_s/l_o and Pr is similar to that reported for a rigid sphere [19].

diffusion. When $\mathrm{Pr}^{-1} \ll l_s/l_o \ll \mathrm{Pr}^{-1/4}$, again the buoyancy forces balance the viscous forces in the matching zone but the density transport is governed by advection. And for $l_s/l_o \gg \mathrm{Pr}^{-1/4}$, the inertia forces balance the viscous forces in the matching zone. In these three regimes, for $u_3 = 1$, the drag simplifies to

$$F_3 = -2\pi\mathcal{R}\begin{cases} 1 + 0.2207\mathcal{R}\,\epsilon & \text{for} \quad l_s/l_o \ll \mathrm{Pr}^{-1}, \\ 1 + 0.3533\mathcal{R}\,\mathrm{Ri}^{1/3} & \text{for} \quad \mathrm{Pr}^{-1} \ll l_s/l_o \ll \mathrm{Pr}^{-1/4}, \\ 1 + (\mathcal{R}/8)\mathrm{Re} & \text{for} \quad l_s/l_o \gg \mathrm{Pr}^{-1/4}. \end{cases} \tag{31}$$

This relationship recovers the result reported for a rigid sphere when $\lambda \to \infty$ (equivalently $\mathcal{R} = 3$) [19]. We can rewrite the correction to drag in terms of Re, Fr, and Pr using $\mathrm{Ri} = \frac{\mathrm{Re}}{\mathrm{Fr}^2}$. We multiply the resulting expression with Re^{-1} to find the drag correction nondimensionalized by $\rho_\infty u_c^2 a^2$. We find that drag correction scales as $(\mathrm{ReFr})^{-1/2}\mathrm{Pr}^{1/4}$ in the diffusive regime and as $(\mathrm{ReFr})^{-2/3}$ in the advective regime. Numerical results of Ref. [16] have also captured these force scales. For $\mathrm{Fr} > \mathrm{Re}^{-1}$, it was noted in Ref. [16] the existence of another scaling regime in which the drag correction scales as $(\mathrm{ReFr})^{-1}$. For these Fr and for any Pr of interest (i.e., $\mathrm{Pr} \leqslant 700$), our calculation holds but we do not see such a scaling regime. Our results also provide the flow field around a settling rigid sphere in a stratified fluid when $\lambda \to \infty$. This solution was not provided in Refs. [18,19].

IV. FLOW FIELD

In this section, we derive the first-order flow fields inside the drop and in the inner zone outside the drop, which will be used in the next section to determine the drop deformation. These flows can be combined with the leading-order flows in both zones to determine a uniform approximation to the flow field. Generally, we need the entire leading-order flow in the outer zone to determine the required first-order flows. But in this problem, we see that only the uniform part of the leading-order flow in the outer zone $\mathscr{T}_1'$ is sufficient to determine the required flows.

After substituting the expansion (18) in Eqs. (7), (8), (10), and (11), collecting the terms of order ϵ, and expressing the velocity fields in terms of stream functions [Eq. (32)], we find that at first

order, the stream function inside the drop $\psi_{1,d}$ and that in the inner zone outside the drop ψ_1' are governed by Eqs. (33) and (34),

$$w_{1,r}' = -\frac{1}{r^2}\frac{\partial \psi_1'}{\partial \eta}, \quad w_{1,\theta}'\sqrt{1-\eta^2} = -\frac{1}{r}\frac{\partial \psi_1'}{\partial r}, \quad \text{where} \quad \eta = \cos\theta, \tag{32}$$

$$E^4 \psi_{1,d} = 0, \tag{33}$$

$$E^4 \psi_1' = 3\mathcal{R}u_3^2 \frac{l_s}{l_o}\left\{\frac{1}{r^2} - \frac{1}{2r^3}\left(\frac{3\lambda+2}{\lambda+1}\right) + \frac{1}{2r^5}\frac{\lambda}{\lambda+1}\right\} Q_2(\eta). \tag{34}$$

Here $E^2 = \frac{\partial^2}{\partial r^2} + \frac{(1-\eta^2)}{r^2}\frac{\partial^2}{\partial \eta^2}$, $Q_n(\eta) = \int_{-1}^{\eta} P_n(\xi)\, d\xi$, and P_n is the Legendre polynomial of degree n. The conditions of zero normal velocity on the drop surface, the continuity of tangential velocity, and the shear stress across the drop surface and the axisymmetricity of velocity fields can be expressed in terms of stream functions as follows:

$$\psi_1'\big|_{r=1} = \psi_{1,d}\big|_{r=1} = 0, \tag{35}$$

$$\left.\frac{\partial \psi_1'}{\partial r}\right|_{r=1} = \left.\frac{\partial \psi_{1,d}}{\partial r}\right|_{r=1}, \tag{36}$$

$$\left.\frac{\partial}{\partial r}\left(\frac{1}{r^2}\frac{\partial \psi_1'}{\partial r}\right)\right|_{r=1} = \lambda \left.\frac{\partial}{\partial r}\left(\frac{1}{r^2}\frac{\partial \psi_{1,d}}{\partial r}\right)\right|_{r=1}, \tag{37}$$

$$\begin{aligned} \psi_1' &= 0 \text{ along } \eta = \pm 1 \text{ and } r \geqslant 1, \\ \psi_{1,d} &= 0 \text{ along } \eta = \pm 1 \text{ and } r \leqslant 1. \end{aligned} \tag{38}$$

The general solution of Eq. (34) that satisfies the zero stream function on the drop surface and along the axis of symmetry is

$$\begin{aligned} \psi_1' = u_3^2 \frac{l_s}{l_o}\frac{\mathcal{R}}{8}\left\{r^2 - \frac{r}{2}\left(\frac{3\lambda+2}{\lambda+1}\right) + \frac{\lambda}{\lambda+1} - \frac{1}{2r}\left(\frac{\lambda}{\lambda+1}\right)\right\} Q_2(\eta) \\ + \sum_{n=1}^{\infty} \{A_n(r^{n+3} - r^{-n}) + B_n(r^{n+1} - r^{-n}) + C_n(r^{2-n} - r^{-n})\} Q_n(\eta). \end{aligned} \tag{39}$$

Using a relation similar to Eq. (32) between the leading-order stream function in the inner zone ψ_0' and the flow field $\mathbf{w}'_0$, we find that ψ_0' is given by

$$\psi_0' = -\frac{u_3}{2}\left[\mathcal{R}r - \left(\frac{\lambda}{\lambda+1}\right)\frac{1}{r}\right] Q_1(\eta). \tag{40}$$

In the matching zone $r \gg 1$, we have

$$\psi_0' + \epsilon\psi_1' = -\frac{\mathcal{R}}{2}u_3 r Q_1(\eta) + \epsilon \frac{l_s}{l_o}u_3^2\frac{\mathcal{R}}{8}r^2 Q_2(\eta) + \epsilon \sum_{n=1}^{\infty}\{A_n r^{n+3} + B_n r^{n+1}\} Q_n(\eta) + O(\epsilon r). \tag{41}$$

Again using a relation similar to Eq. (32), we connect the flow fields in the outer zone $\mathscr{T}_0'$, $\mathscr{T}_1'$ to the stream functions Ψ_0', Ψ_1', in turn deriving the following expressions for the stream functions:

$$\Psi_0' = -\frac{\mathcal{R}}{2}u_3 r Q_1(\eta), \quad \Psi_1' = \frac{\mathcal{R}}{3}M_{33,\text{rgsp}}u_3 r^2 Q_1(\eta), \tag{42}$$

$$\Rightarrow \Psi_0' + \epsilon\,\Psi_1' = \left(-\frac{\mathcal{R}}{2}u_3 r + \epsilon\frac{\mathcal{R}}{3}M_{33,\text{rgsp}}u_3 r^2\right) Q_1(\eta). \tag{43}$$

We now match Eq. (41) with Eq. (43) in the matching zone $r \gg 1$. For this purpose, we require that ψ_1' does not grow faster than r^2 and that the coefficient of $r^2 Q_1(\eta)$ is the same in these two equations. These conditions are satisfied provided

$$A_n = 0 \text{ for } n \geqslant 1, \quad B_n = 0 \text{ for } n \geqslant 2, \quad \text{and} \quad B_1 = \frac{\mathcal{R}}{3} M_{33,\text{rgsp}} u_3. \tag{44}$$

We cannot match the term $\epsilon \frac{l_s}{l_o} u_3^2 \frac{\mathcal{R}}{8} r^2 Q_2(\eta)$ in $\psi_0' + \epsilon \psi_1'$ with any of the terms in $\Psi_0' + \epsilon\, \Psi_1'$. This is expected as the term $\frac{l_s}{l_o} u_3^2 \frac{\mathcal{R}}{8} r^2 Q_2(\eta)$ in ψ_1' represents a nonuniform flow that cannot be matched with the (only found) uniform flow part of the leading-order flow (minus the Stokeslet) in the outer zone.

The solution of Eq. (33), which ensures that the stream function will be zero on the drop surface and along the axis of symmetry and which gives finite velocities at the drop center, is

$$\psi_{1,d} = \sum_{n=1}^{\infty} A_{n,d} (r^{n+3} - r^{n+1}) Q_n(\eta). \tag{45}$$

We now enforce the conditions (36) and (37) on ψ_1' and $\psi_{1,d}$ to determine the remaining unknown constants C_n and $A_{n,d}$, whose expressions are given as

$$\begin{aligned} C_1 &= -\frac{\mathcal{R}^2 u_3}{6} M_{33,\text{rgsp}}, \quad C_2 = -\frac{l_s}{l_o} \frac{u_3^2}{80} \frac{\mathcal{R}\lambda(5\lambda+6)}{(\lambda+1)^2}, \\ A_{1,d} &= \frac{\mathcal{R} u_3}{6} \frac{M_{33,\text{rgsp}}}{(\lambda+1)}, \quad A_{2,d} = \frac{l_s}{l_o} \frac{u_3^2}{80} \frac{\mathcal{R}(4\lambda+5)}{(\lambda+1)^2}, \\ C_n &= A_{n,d} = 0 \quad \text{for} \quad n \geqslant 3. \end{aligned} \tag{46}$$

As the first-order drag acting on the drop is given by [38] $4\pi C_1\, \mathbf{e}_3 = -\frac{2\pi}{3} \mathcal{R}^2 u_3 M_{33,\text{rgsp}}\, \mathbf{e}_3$, this validates the drag determined in the previous section without calculating the flow field. Using Eqs. (44) and (46), the expressions for the first-order stream functions inside the drop and in the inner zone outside the drop are given as

$$\psi_{1,d} = -\frac{\mathcal{R}}{2(\lambda+1)} \left\{ \frac{M_{33,\text{rgsp}} u_3}{3} (r^2 - r^4) Q_1(\eta) + \frac{l_s}{l_o} \frac{(4\lambda+5)}{40(\lambda+1)} u_3^2 (r^3 - r^5) Q_2(\eta) \right\}, \tag{47}$$

$$\begin{aligned} \psi_1' = {} & \frac{\mathcal{R}}{3} M_{33,\text{rgsp}} u_3 \left\{ r^2 - \frac{\mathcal{R}}{2} r + \frac{1}{2r} \left(\frac{\lambda}{\lambda+1} \right) \right\} Q_1(\eta) \\ & + \frac{\mathcal{R}}{8} \frac{l_s}{l_o} u_3^2 \left\{ r^2 - \frac{\mathcal{R}}{2} r + \frac{1}{10} \frac{\lambda(5\lambda+4)}{(\lambda+1)^2} - \frac{1}{2r} \left(\frac{\lambda}{\lambda+1} \right) + \frac{1}{10} \frac{\lambda(5\lambda+6)}{(\lambda+1)^2} \frac{1}{r^2} \right\} Q_2(\eta). \end{aligned} \tag{48}$$

From these calculations, we notice that the stratification modifies the flow field close to the drop at $O(\epsilon)$, so the flow field close to the drop in a stratified fluid should be approximately the same as that in a homogeneous fluid. We also infer that the stratification should alter the flow field far away from the drop in a significant manner because unlike the inner zone, the influence of stratification is felt at the leading order in the outer zone. By looking at the equations governing flow field in the outer zone, Eqs. (19)–(21), we see that this flow is essentially the flow due to a point force singularity placed in a stratified fluid, which was already analyzed by Ardekani and Stocker [35] in the limit $\text{Pe} \ll \epsilon$ or $l_s/l_o \ll \text{Pr}^{-1}$. Hence, the flow field far away from the drop in a stratified fluid should be a Stratlet flow field. Most of these deductions are consistent with Fig. 3, where we plotted the streamlines associated with the composite expansion of flow field accurate to $O(\epsilon)$ for $\text{Pe} \ll \epsilon$, $\lambda = 1$, and $\epsilon = 0.1$. From Fig. 3(b), we see that the flow field far away from the drop in a stratified fluid is not a Stratlet flow field. This is because, at these distances from the drop, the

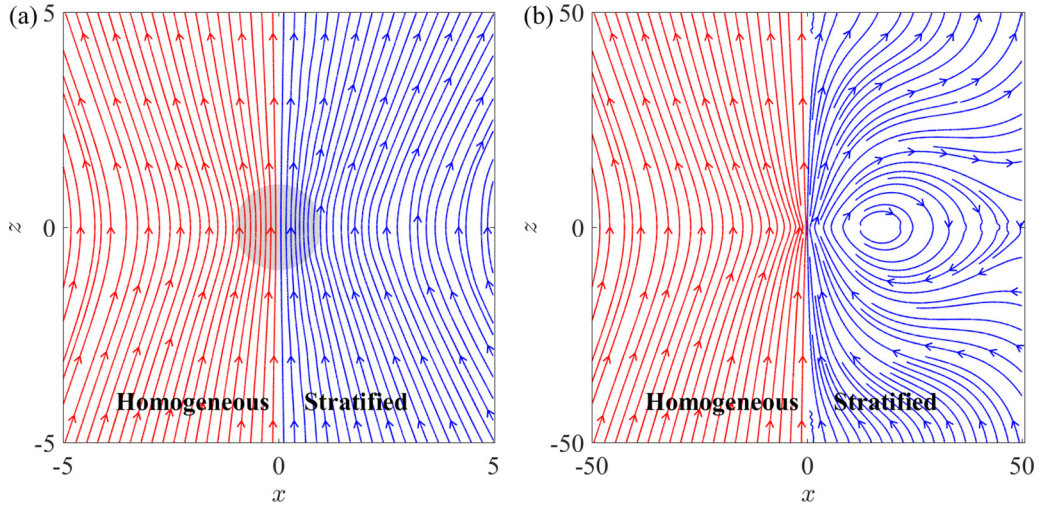

FIG. 3. In the laboratory frame of reference, we compare the streamlines in a homogeneous fluid (red lines) with those in a stratified fluid (blue lines) both near the drop (a) and far away from it (b). The streamlines in a stratified fluid are determined from the composite expansion of flow field accurate to $O(\epsilon)$ at $\mathrm{Pe} \ll \epsilon$, $\lambda = 1$, and $\epsilon = 0.1$. To find this composite expansion, we combined the flow fields in the inner zone and the outer zone in the usual manner [44], where the flow in the outer zone is determined by doing an inverse Fourier transform of Eq. (23) using the FFT package of MATLAB [45].

Stokeslet contribution of the first-order inner flow field is significant enough to alter the expected Stratlet flow field. We expect to recover the Stratlet flow at even farther distances from the drop.

V. DROP DEFORMATION

In this section, we determine the leading-order deformation of a drop rising in a stratified fluid. For this purpose, we consider the normal stress balance condition on the drop surface, and we solve for the deformation knowing the flow field inside and outside but close to the drop. The dimensionless normal stress boundary condition is given by

$$\left\{\begin{array}{l}\left[\lambda p'_d - p' + 2\frac{\partial w'_r}{\partial r} - 2\lambda\frac{\partial w_{d,r}}{\partial r}\right]_{r=1} \\ +\frac{ga^2\eta}{\nu u_c}\left(1 - \frac{\gamma a}{\rho_\infty}x_{d,3} - \alpha\right) - \frac{\epsilon^3}{2\frac{l_s}{l_o}\,\mathrm{Pr}}\eta^2\end{array}\right\} = \frac{1}{\mathrm{Ca}}(\nabla\cdot\mathbf{n}) = \frac{1}{\mathrm{Ca}}\left\{2 - 2\zeta - \frac{d}{d\eta}\left[(1-\eta^2)\frac{d\zeta}{d\eta}\right]\right\}. \quad (49)$$

As the term $\frac{\epsilon^3}{2\frac{l_s}{l_o}\,\mathrm{Pr}}\eta^2$ is much smaller than the remaining terms on the left-hand side of Eq. (49), and also since we are only interested in finding the leading-order drop deformation, we neglect this term. Here $x_{d,3} = \mathbf{x}_d \cdot \mathbf{e}_3$, $\mathrm{Ca} = \rho_\infty \nu u_c/\sigma$ is the Capillary number, which is the ratio of bulk viscous forces to the capillary forces, $\alpha = \frac{\rho_d}{\rho_\infty} = \frac{\lambda}{\chi}$ is the density ratio, and we assumed the drop's shape to be $r = 1 + \zeta(\eta)$, $\max|\zeta| \ll 1$ in evaluating the curvature term.

We first evaluate the normal stress boundary condition accurate to $O(1)$ to find the drop deformation accurate to $O(\mathrm{Ca})$. For this purpose, we simply substitute the leading-order pressure fields inside the drop and in the inner zone outside the drop [see Eq. (50)], the corresponding radial

derivative of flow fields [see Eq. (51)] into Eq. (49), and we simplify it to obtain Eq. (52),

$$p'_{0,d}|_{r=1} = -\frac{5}{(\lambda+1)}u_3\eta + c_{0,d}, \quad p'_0|_{r=1} = \frac{1}{2}\left(\frac{3\lambda+2}{\lambda+1}\right)u_3\eta + c_0, \tag{50}$$

$$\left.\frac{\partial w_{0,d,r}}{\partial r}\right|_{r=1} = \left.\frac{\partial w'_{0,r}}{\partial r}\right|_{r=1} = -\frac{u_3\eta}{(\lambda+1)}, \tag{51}$$

$$\eta\left[\frac{ga^2}{\nu u_c}\left(1-\frac{\gamma a}{\rho_\infty}x_{d,3}-\alpha\right)-\frac{3\mathcal{R}u_3}{2}\right]+\Pi_0 = \frac{1}{\mathrm{Ca}}\left\{2-2\zeta-\frac{d}{d\eta}\left[(1-\eta^2)\frac{d\zeta}{d\eta}\right]\right\}. \tag{52}$$

Here c_0, $c_{0,d}$, and $\Pi_0 = \lambda c_{0,d} - c_0$ are constants.

As the drop is undergoing quasisteady motion, the net force acting on it should be zero. The drop experiences three kinds of forces—buoyancy, drag, and its own weight. The buoyancy can be found by integrating the hydrostatic pressure acting on the drop i.e., $-\int_{r=1} p_0 \mathbf{n} dS = (1-\frac{\gamma a}{\rho_\infty}x_{d,3})\frac{ga^2}{\nu u_c}\int_{r=1} r_3\mathbf{n}dS - \frac{\epsilon^3}{2\frac{l_s}{l_o}\mathrm{Pr}}\int_{r=1} r_3^2\mathbf{n}dS = \frac{4\pi}{3}(1-\frac{\gamma a}{\rho_\infty}x_{d,3})\frac{ga^2}{\nu u_c}\mathbf{e}_3$, where the last simplification is done using $\int_{r=1} r_3\mathbf{n}dS = \frac{4\pi}{3}\mathbf{e}_3$ and $\int_{r=1} r_3^2\mathbf{n}dS = \mathbf{0}$. Using this expression for buoyancy, Eq. (29) for drag, and the usual expression for the drop's weight, the force balance condition simplifies to

$$\frac{ga^2}{\nu u_c}\left(1-\frac{\gamma a}{\rho_\infty}x_{d,3}-\alpha\right)-\frac{3\mathcal{R}u_3}{2} = \frac{\epsilon\mathcal{R}^2}{2}M_{33,\mathrm{rgsp}}u_3. \tag{53}$$

This condition is accurate to $O(\epsilon)$ and we can simply set the right-hand side to zero to find the force balance condition at $O(1)$.

We now simplify the leading-order normal stress boundary condition, Eq. (52), using the force balance condition at $O(1)$ to obtain

$$\Pi_0 = \frac{1}{\mathrm{Ca}}\left\{2-2\zeta-\frac{d}{d\eta}\left[(1-\eta^2)\frac{d\zeta}{d\eta}\right]\right\}. \tag{54}$$

Enforcing the constraints that the drop's volume does not change, $\int_{-1}^{1}\zeta(\eta)d\eta = 0$, and its center of mass remains fixed, $\int_{-1}^{1}\eta\zeta(\eta)d\eta = 0$, during the process of deformation, we find that the deformation is zero, i.e., $\zeta = 0$, while $\Pi_0 = 2/\mathrm{Ca}$. This is not surprising because at $O(1)$, the stratification and inertia do not affect the flow, and we have a drop rising in a homogeneous fluid at zero Re, which was shown not to deform [37,38].

To determine the effect of inertia and stratification on drop deformation, we evaluate the normal stress boundary condition accurate to $O(\epsilon)$. To do so, we substitute Eqs. (50), (51), and (55)–(57) in Eq. (49) and simplify it to obtain Eq. (58),

$$\begin{aligned} p'_{1,d}|_{r=1} = {} & \frac{l_s}{l_o}\frac{\alpha {u_3}^2}{24(\lambda+1)^2\lambda} + c_{1,d} - \frac{5(3\lambda+2)M_{33,\mathrm{rgsp}}u_3}{3(\lambda+1)^2}P_1(\eta) \\ & + \frac{l_s}{l_o}\frac{{u_3}^2(-252\lambda^3+20\lambda\alpha-483\lambda^2+20\alpha-210\lambda)}{240\lambda(\lambda+1)^3}P_2(\eta), \end{aligned} \tag{55}$$

$$\begin{aligned} p'_1|_{r=1} = {} & -\frac{l_s}{l_o}\frac{\left(\lambda^2+2\lambda+\frac{4}{3}\right){u_3}^2}{16(\lambda+1)^2} + c_1 + \frac{(3\lambda+2)^2M_{33,\mathrm{rgsp}}u_3}{6(\lambda+1)^2}P_1(\eta) \\ & + \frac{l_s}{l_o}\frac{{u_3}^2(135\lambda^3+333\lambda^2+272\lambda+80)}{240(\lambda+1)^3}P_2(\eta), \end{aligned} \tag{56}$$

$$\left.\frac{\partial w_{1,d,r}}{\partial r}\right|_{r=1} = \left.\frac{\partial w'_{1,r}}{\partial r}\right|_{r=1} = -\frac{(3\lambda+2)M_{33,\mathrm{rgsp}}u_3}{3(\lambda+1)^2}P_1(\eta) - \frac{l_s}{l_o}\frac{(3\lambda+2)(4\lambda+5){u_3}^2}{40(\lambda+1)^3}P_2(\eta), \tag{57}$$

$$\left\{\begin{array}{l}\eta\left[\frac{ga^2}{\nu u_c}\left(1-\frac{\gamma a}{\rho_\infty}x_{d,3}-\alpha\right)-\frac{3\mathcal{R}u_3}{2}-\frac{\epsilon\mathcal{R}^2}{2}M_{33,\mathrm{rgsp}}u_3\right]\\ +\Pi_0+\epsilon\left[\Pi_1+\frac{l_s}{l_o}\frac{u_3^2}{48}\frac{(3\lambda^2+2\alpha+6\lambda+4)}{(\lambda+1)^2}\right]\\ +\epsilon\frac{l_s}{l_o}\frac{u_3^2}{240}\frac{\begin{pmatrix}-243\lambda^3+20\alpha\lambda-684\lambda^2\\+20\alpha-638\lambda-200\end{pmatrix}}{(\lambda+1)^3}P_2(\eta)\end{array}\right\}=\frac{1}{\mathrm{Ca}}\left\{2-2\zeta-\frac{d}{d\eta}\left[(1-\eta^2)\frac{d\zeta}{d\eta}\right]\right\}. \quad (58)$$

Here c_1, $c_{1,d}$, and $\Pi_1=\lambda c_{1,d}-c_1$ are constants. We note that only the first term on the left-hand side of Eq. (58) that is proportional to η contains the information of stratification through this term's dependence on $M_{33,\mathrm{rgsp}}$. But this term is identically zero due to the force balance condition accurate to $O(\epsilon)$, Eq. (53), making the drop deformation independent of stratification. Using $\Pi_0=2/\mathrm{Ca}$ and the force balance condition accurate to $O(\epsilon)$, Eq. (58) simplifies to

$$\left\{\begin{array}{l}\epsilon\left[\Pi_1+\frac{l_s}{l_o}\frac{u_3^2}{48}\frac{(3\lambda^2+2\alpha+6\lambda+4)}{(\lambda+1)^2}\right]\\ +\epsilon\frac{l_s}{l_o}\frac{u_3^2}{240}\frac{\begin{pmatrix}-243\lambda^3+20\alpha\lambda-684\lambda^2\\+20\alpha-638\lambda-200\end{pmatrix}}{(\lambda+1)^3}P_2(\eta)\end{array}\right\}=-\frac{1}{\mathrm{Ca}}\left\{2\zeta+\frac{d}{d\eta}\left[(1-\eta^2)\frac{d\zeta}{d\eta}\right]\right\}. \quad (59)$$

We solve this equation for the drop deformation by making sure the drop's volume and its center of mass remain fixed during the process of deformation to obtain

$$\zeta(\eta)=\frac{\mathrm{We}\,u_3^2}{960}\frac{(-243\lambda^3+20\alpha\lambda-684\lambda^2+20\alpha-638\lambda-200)}{(\lambda+1)^3}P_2(\eta), \quad (60)$$

where the Weber number $\mathrm{We}=\mathrm{Re}\,\mathrm{Ca}$. We note that this is exactly the deformation of a drop rising in a homogeneous fluid at small Re [37,38], in which case the drop deforms into an oblate spheroid. Hence, the stratification does not affect the drop's deformation to this order of approximation. To understand this observation, let us see how inertia or stratification modifies the flow field in the inner zone. Let us first consider the case of zero inertia. The effect of stratification is to induce a uniform flow far away from drop, due to which at $O(\epsilon)$ we have a stationary drop placed in a homogeneous fluid that is undergoing uniform streaming flow far away from the drop. As this problem is the same as the drop moving in a homogeneous quiescent fluid at zero Re, with a change of reference frames, we expect the drop not to deform. Now, if we include inertia, it has two effects. It modifies the strength of uniform flow far away from the drop, which again does not cause any drop deformation. It also induces a nonuniform flow everywhere in the domain due to the particular integral of Eq. (34), and this is the sole cause of drop deformation.

The leading-order effect of deformation on the drag can be found by simply considering the deformed drop in a creeping flow of a homogeneous fluid [37]. As the stratification does not cause any deformation of the drop, this deformation induced change in the drag is the same as that found for a drop motion in a homogeneous fluid at small Re [37]. Briefly, this modification in the drag is $O(\mathrm{We})$, and since $\mathrm{We}=(\frac{\rho_\infty\nu^2}{a\sigma})\mathrm{Re}^2\sim O(\epsilon^2)$, we conclude that the deformation affects the drag at $O(\epsilon^2)$. But we do not include this deformation induced drag in Eq. (29) because for consistent asymptotic expansion of drag accurate to $O(\epsilon^2)$, we also need to find $O(\epsilon^2\ln\epsilon)$ drag, whose calculation is beyond the scope of this work. We expect a nonzero drag at $O(\epsilon^2\ln\epsilon)$ based on the calculations for the motion of a drop in a homogeneous fluid at small Re [37,46].

VI. DRIFT VOLUME

In this section, we calculate the partial drift volume induced by a drop rising in a stratified fluid. Drift volume is the volume enclosed between an initially marked plane of fluid of infinite extent and the deformed plane as the drop travels normal to the initial plane of fluid starting far ahead to

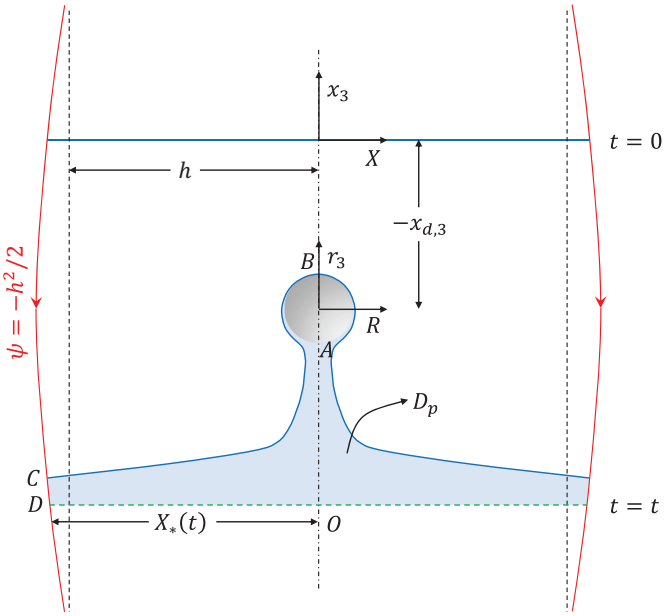

FIG. 4. Schematic showing the definition of the partial drift volume D_p and the coordinate systems involved. In the drop frame, at time $t = 0$, the marked fluid disk (shown by the blue straight line) is located at a distance $-x_{d,3}$ from the drop. At time t, the marked fluid plane deforms (shown by the blue curved line) as it crosses the drop. The area enclosed between the deformed and undeformed marked fluid planes (multiplied by π) gives the partial drift volume D_p at time t (shown by the light blue region).

far beyond the plane of fluid. When both the extent of the marked plane of fluid and the distance traveled by the drop relative to the plane of fluid are finite, the volume encapsulated between the initial and the deformed planes of fluid is referred to as the partial drift volume D_p [28] (see Fig. 4 for a schematic).

To make our notation consistent with earlier works on drift volume, we nondimensionalize velocity using $|u_3|$, time using $a/|u_3|$, and we assume $u_3 > 0$. All the variables that appear in this section are nondimensionalized in this manner. In the present notation, any field variable can be found by simply setting $u_3 = 1$ in the expression of that field variable derived in the previous sections. The marked plane of fluid is a disk of finite radius and zero thickness. In the laboratory frame, we choose the center of disk as the origin, and we denote the cylindrical coordinate variables about this origin by X, x_3. In the frame moving with the drop, we choose the center of the drop as the origin, and we denote the cylindrical coordinate variables about this origin by R, r_3. At time $t = 0$, the marked disk of fluid is located at a distance $-x_{d,3}$ upstream of the drop. Hence, $r_3 = x_3 - (x_{d,3} + t)$ and $R = X$. As far as the flow field outside the drop is concerned, the disturbance flow in the drop frame and the flow field in the laboratory frame are the same. We used ψ' to denote the stream function associated with this flow. We denote the stream function associated with the flow field in the drop frame by ψ. Note that ψ approaches $-R^2/2$ far from the drop and $\psi' = \psi + \frac{X^2}{2}$. The intersection of the streamline $\psi = -h^2/2$ with the plane $x_3 = 0$ gives the extent of marked fluid disk. We denote the point of intersection by $(x_3, X) = (0, X_*(t))$ and the stream function at this point by $\psi'_*(t)$.

In the laboratory frame, we apply the conservation of mass to the control volume (CV) *OABCD*,

$$\frac{\partial}{\partial t}\int_{\mathrm{CV}} \rho \, dV + \int_{\mathrm{CS}} \rho \, \mathbf{w}' \cdot \mathbf{n} \, dS = 0, \tag{61}$$

where CS denotes the control surface bounding the CV. We choose the surfaces AB, BC, and CD as the material surfaces, and since OA is a streamsurface, $\mathbf{w}' \cdot \mathbf{n}$ is nonzero only along the surface OD. Hence, the conservation of mass simplifies to

$$\frac{\partial}{\partial t}\int_{\mathrm{CV}} \rho\, dV + \int_{OD} \rho\, \mathbf{w}' \cdot \mathbf{n}\, dS = 0. \tag{62}$$

In the context of the Boussinesq approximation, ρ can be treated as constant in the conservation of mass. So, after integration with respect to time and expressing velocity in terms of stream function, we have

$$D_p = 2\pi \int_0^t \psi'_*(t')\, dt' - [V_b(t) - V_b(0)]. \tag{63}$$

This expression for D_p is the same as that found in a homogeneous fluid [28] and it says that the partial drift volume at time t is equal to the volume of fluid that has passed through the plane $x_3 = 0$ bounded by the streamline $\psi = -h^2/2$ by time t. Here $V_b(t)$ denotes the volume of the drop that has crossed the plane $x_3 = 0$ by time t. Assuming the extent of the marked fluid disk is large compared to the drop, we neglect the deflection of streamlines and set $X_* = h$, hence $\psi'_*(t) = \psi'(x_3 = 0, X = h, t) = \psi'(r_3 = -(x_{d,3} + t), R = h, t)$. Defining $\tau = (x_{d,3} + t)/h$ and $\tau_0 = x_{d,3}/h$, we obtain

$$D_p = 2\pi h \int_{\tau_0}^{\tau} \psi'_*(\tau')\, d\tau' - [V_b(\tau) - V_b(\tau_0)]. \tag{64}$$

As D_p is at least $O(h)$, we neglect the $O(1)$ terms in the brackets. Also, as the partial drift volume depends on the stream function far from the drop $\psi'_*(t)$, we simply use the stream function in the outer zone to evaluate D_p. We can show that D_p is $O(h^2)$ and the error in using the flow field in the outer zone to evaluate D_p is $O(h)$ and hence is negligible compared to D_p.

Other than τ and τ_0, $D_p/(\mathcal{R}h^2)$ depends only on $\xi_h = \xi h$ for the values of l_s/l_o given below,

$$\xi = \begin{cases} \epsilon & \text{for} \quad l_s/l_o \ll \mathrm{Pr}^{-1}, \\ \mathrm{Ri}^{1/3} & \text{for} \quad \mathrm{Pr}^{-1} \ll l_s/l_o \ll \mathrm{Pr}^{-1/4}, \\ \mathrm{Re} & \text{for} \quad l_s/l_o \gg \mathrm{Pr}^{-1/4}. \end{cases} \tag{65}$$

$\mathrm{Re}_h = \mathrm{Re}h$ is the ratio of marked disk radius (h) to the distance from the sphere at which inertia forces balance viscous forces. On the other hand, $\epsilon_h = \epsilon h$ (resp. $\mathrm{Ri}_h{}^{1/3} = \mathrm{Ri}^{1/3}h$) is the ratio of marked disk radius to the distance from the sphere at which buoyancy forces balance the viscous forces for low values of Pe (resp. for high values of Pe).

To simplify Eq. (64) for the partial drift volume, we restrict our attention to one of the regimes mentioned in Eq. (65). In this case, we can rescale the variables in the outer zone as $\bar{r} = \xi r$, $\mathbf{w}' = \xi \bar{\mathbf{w}}'$, $p' = \xi^2 \bar{p}'$, $\bar{\psi}' = \xi \psi'$ and solve Eqs. (19)–(21) in Fourier space. Unlike the Fourier and inverse Fourier transforms mentioned in Sec. III, in this section the Fourier transforms involve rescaled coordinate variables, i.e.,

$$\hat{\bar{\psi}}'(\mathbf{k}) = \int d\bar{\mathbf{r}}\, \bar{\psi}'(\bar{\mathbf{r}})\, e^{-i\mathbf{k}\cdot\bar{\mathbf{r}}} \quad \text{and} \quad \bar{\psi}'(\bar{\mathbf{r}}) = \frac{1}{8\pi^3}\int d\mathbf{k}\, \hat{\bar{\psi}}'(\mathbf{k})\, e^{i\mathbf{k}\cdot\bar{\mathbf{r}}}. \tag{66}$$

After finding the Fourier transform of $\bar{\mathbf{w}}'$, namely $\hat{\bar{\mathbf{w}}}'$, we can calculate $\hat{\bar{\psi}}'$ using

$$\hat{\bar{\psi}}'(\mathbf{k}) = -\frac{1}{k_3}\left(\frac{\partial \hat{\bar{w}}'_1}{\partial k_1} + \frac{\partial \hat{\bar{w}}'_2}{\partial k_2}\right). \tag{67}$$

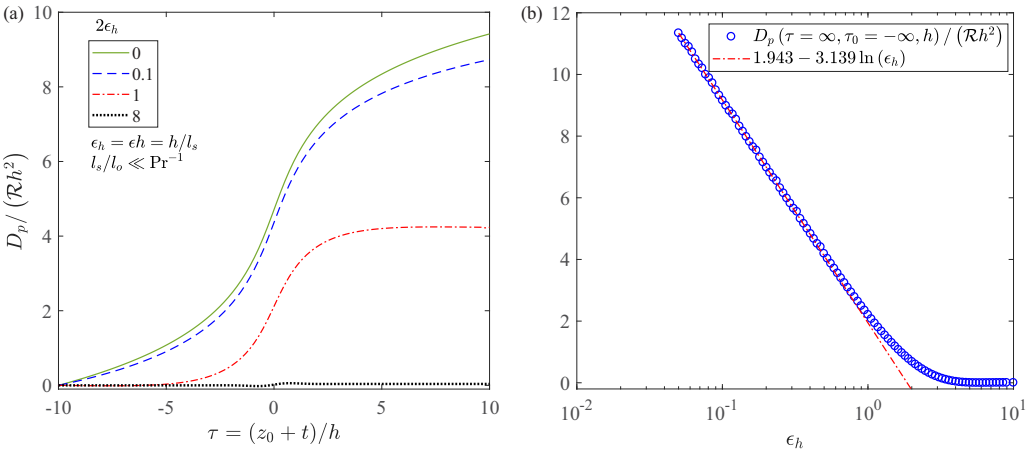

FIG. 5. (a) The variation of $D_p/(\mathcal{R}h^2)$ with τ for $\tau_0 = -10$ and $2\epsilon_h = 0$, 0.1, 1, and 8. (b) In the limit $\tau_0 \to -\infty$ and $\tau \to \infty$, the variation of $D_p/(\mathcal{R}h^2)$ with ϵ_h. Also shown is a fit to the data for $\epsilon_h \leqslant 1$.

Rewriting the inverse Fourier transform in cylindrical coordinates and integrating along the azimuthal direction, we obtain

$$\begin{aligned}\psi'_*(t) &= \psi'(r_3 = -(x_{d,3} + t), R = h, t)\\ &= \frac{1}{4\pi^2\xi}\int_{-\infty}^{\infty} dk_3 \int_0^{\infty} dk_r\, \hat{\hat{\psi}}'(k_r, k_3)\, e^{-ik_3\xi(x_{d,3}+t)}\, k_r J_0(\xi h k_r) dk_r dk_3. \end{aligned} \tag{68}$$

Here, $k_r = \sqrt{{k_1}^2 + {k_2}^2}$, J_0 is the Bessel function of the first kind and zeroth order, and a factor of $1/\xi$ appears due to the relation $\psi' = \bar{\psi}'/\xi$. Rewriting Eq. (68) in terms of τ, substituting for $\psi'_*(\tau')$ in Eq. (64), changing the order of integration, and integrating first with respect to τ', we obtain the expression for D_p as

$$D_p = -\frac{ih^2}{2\pi\xi_h^2}\int_{-\infty}^{\infty} dk_3 \int_0^{\infty} dk_r\, \hat{\hat{\psi}}'(k_r, k_3)\, J_0(\xi_h k_r)\, \frac{(e^{-i\xi_h k_3 \tau_0} - e^{-i\xi_h k_3 \tau})}{k_3}. \tag{69}$$

We can compute this double integral using the integral2 command in MATLAB.

The partial drift volume formula [Eq. (69)] is valid in any of the three regimes mentioned in Eq. (65). The drift volume for the inertia dominant regime ($l_s/l_o \gg \mathrm{Pr}^{-1/4}$) was calculated in Ref. [28]. As the flow field characteristics in the diffusion dominant regime ($l_s/l_o \ll \mathrm{Pr}^{-1}$) were already reported by Ardekani and Stocker [35], we restrict the drift volume calculation to this regime only. In this case, $\hat{\hat{\psi}}'(k_r, k_3)$ is given by

$$\hat{\hat{\psi}}' = \frac{4\pi\mathcal{R}\left(k_3^8 + 2k_3^6 k_r^2 - 2k_3^2 k_r^6 - k_r^8 + k_r^4\right)}{\left(k_3^6 + 3k_3^4 k_r^2 + 3k_3^2 k_r^4 + k_r^6 + k_r^2\right)^2}. \tag{70}$$

We plot the variation of D_p with τ and ϵ_h at $\tau_0 = -10$ in Fig. 5(a). For a fixed value of h, an increase in ϵ_h is equivalent to an increase in ϵ or the stratification. This increases the tendency of the perturbed isopycnals (due to the passage of drop) to return to their unperturbed level, which reduces the drift volume. As $\hat{\hat{\psi}}'(k_r, k_3)$ is even in k_3, the flow field is fore-aft symmetric. As a result, the upstream drift volume is equal to the downstream drift volume, i.e., $D_p(\tau, \tau_0 = 0, h) = -D_p(\tau = -\tau, \tau_0 = 0, h)$. The fore-aft symmetry of the flow can also be seen from the flow-field plots [see Fig. 3 here and Fig. 1(b) in Ref. [35]]. Also, as D_p is $O(h^2)$ or at least $O(h) \gg 1$, the drop drags a huge volume of fluid in comparison to its own volume as it rises in a stratified fluid.

We note that the flow field due to a point force (far-field representation of a drop) in a stratified fluid is qualitatively similar to the flow due to a point force in a homogeneous fluid but bounded by walls [35]. As the drift volume induced by a sphere moving in a homogeneous fluid near the wall is reported to achieve a constant value [27], we expect the drift volume induced by a drop rising in a stratified fluid to also achieve a constant value that is a function of ϵ_h. We plot the drift volume or the asymptotic value of D_p in the limit $\tau_0 \to -\infty$ and $\tau \to \infty$ in Fig. 5(b) as a function of ϵ_h. Here, we see that for $\epsilon_h \leqslant 1$, the drift volume is proportional to $\ln(\epsilon_h)$.

The time that the partial drift volume takes to attain the constant asymptotic value is inversely proportional to ϵ_h. In the limit $\epsilon_h \to 0$, the partial drift volume takes infinite time to achieve this asymptotic value or such a constant drift volume is never achieved. This makes sense, as in this limit the inner region approaches infinity, so the entire fluid is homogeneous, in which case the partial drift volume diverges with time. We note that in the limit $\epsilon_h \to 0$, we can treat the fluid in the inner zone as homogeneous as far as the partial drift volume calculation is concerned because the first-order flow in the inner zone does not contribute to the leading-order partial drift volume.

VII. CONCLUSIONS

For a drop rising in a linearly density stratified fluid, we calculated the drag, deformation, and drift volume induced by the drop, and the flow field surrounding the drop. We assumed the drop has a constant density and uniform interfacial tension. Our calculations of drag, deformation, and flow field are valid when the inertia and stratification effects are small (but not negligible), the kinematic viscosity ratio $\chi \geqslant 1$, and for arbitrary values of the Prandtl number Pr and the dynamic viscosity ratio λ. For the Reynolds number $\mathrm{Re} \approx 0.1$, this corresponds to the Froude number $\mathrm{Fr} \gg 0.08$ for the temperature stratified air, $\mathrm{Fr} \gg 0.26$ for the temperature stratified water, and $\mathrm{Fr} \gg 2.64$ for the salt stratified water. The drift volume calculation, on the other hand, is valid for small stratification and advective transport rate of density, and negligible inertia.

The combined influence of stratification and inertia is to increase the drag, and this drag enhancement on the drop is equal to $(\frac{3\lambda+2}{3(\lambda+1)})^2$ times the drag enhancement on a rigid sphere. The leading-order effect of stratification is to induce a uniform flow far away from the drop, which does not cause any drop deformation. This leading-order effect of stratification holds even for a sedimenting particle of arbitrary shape due to which the stratification does not generate any hydrodynamic torque on a nonskew particle [47]. In a stratified fluid, the return of perturbed isopycnals to their unperturbed level causes a reflux of fluid, which reduces the partial drift volume induced by the drop. This in turn causes the drop to induce a finite drift volume (yet large compared to the drop's volume) in a stratified fluid unlike an infinite drift volume induced in a homogeneous fluid. Our study is a theoretical calculation of drift volume induced by objects (drop or rigid sphere) in a density stratified fluid, and this calculation is valuable in the context of the ongoing debate in the literature on biogenic mixing in the oceans.

Prior to our calculation, it was known that a rising drop in a homogeneous fluid at zero inertia is the only situation in which the drop does not exhibit any deformation [38]. In all other problems concerned with drop motion, the drop deforms. Through our calculation, we discovered an additional scenario in which the drop does not deform—a rising drop in a density stratified fluid at zero inertia. It is then interesting to find out if a drop of arbitrary shape would evolve to a spherical shape after a long time. This problem is essentially identifying the stability of a spherical shape for a drop rising in a density stratified fluid at zero inertia, for both infinitesimal [48] and finite [49] perturbations from the sphere.

In the event of an oil spill, surfactants are usually added to break down the heavier oil components into small drops. These drops are always surrounded by marine microbes as they serve as nutrient sources for the microbes. To understand the bioremediation of an oil spill by marine microbes, in an earlier work we solved this problem without considering the effects of density stratification by modeling the microbe as a force-dipole and using the method of images to study the hydrodynamic

interaction between drops and nearby microbes [50–53]. We can now borrow the ideas from the present work to understand how density stratification modifies the interaction of microbes with drops rising in density stratified oceans.

ACKNOWLEDGMENTS

This work is partially supported by the National Science Foundation Grants No. NSF CBET-1604423 and No. NSF CBET-1705371. V.A.S. thanks the Bilsland Dissertation Fellowship for the financial support.

[1] D. F. Hill, A. M. Vergara, and E. J. Parra, Destratification by mechanical mixers: Mixing efficiency and flow scaling, J. Hydraul. Eng. **134**, 1772 (2008).
[2] M. Blumer, H. L. Sanders, J. F. Grassle, and G. R. Hampson, An ocean of oil: A small oil spill, Environment: Sci. Policy Sustainable Devel. **13**, 2 (1971).
[3] A. M. Ardekani, A. Doostmohammadi, and N. Desai, Transport of particles, drops, and small organisms in density stratified fluids, Phys. Rev. Fluids **2**, 100503 (2017).
[4] J. Magnaudet and M. J. Mercier, Particles, drops, and bubbles moving across sharp interfaces and stratified layers, Annu. Rev. Fluid Mech. **52**, 61 (2020).
[5] A. N. Srdic-Mitrovic, N. A. Mohamed, and H. J. S. Fernando, Gravitational settling of particles through density interfaces, J. Fluid Mech. **381**, 175 (1999).
[6] N. Abaid, D. Adalsteinsson, A. Agyapong, and R. M. McLaughlin, An internal splash: Levitation of falling spheres in stratified fluids, Phys. Fluids **16**, 1567 (2004).
[7] R. Camassa, C. Falcon, J. Lin, R. M. McLaughlin, and R. Parker, Prolonged residence times for particles settling through stratified miscible fluids in the Stokes regime, Phys. Fluids **21**, 031702 (2009).
[8] R. Camassa, C. Falcon, J. Lin, R. M. McLaughlin, and N. Mykins, A first-principle predictive theory for a sphere falling through sharply stratified fluid at low Reynolds number, J. Fluid Mech. **664**, 436 (2010).
[9] C. R. Torres, J. Ochoa, J. E. Castillo, and H. Hanazaki, Numerical simulation of flow past a sphere in vertical motion within a stratified fluid, J. Comput. Appl. Math. **103**, 67 (1999).
[10] C. R. Torres, H. Hanazaki, J. Ochoa, J. Castillo, and M. Van Woert, Flow past a sphere moving vertically in a stratified diffusive fluid, J. Fluid Mech. **417**, 211 (2000).
[11] H. Hanazaki, K. Konishi, and T. Okamura, Schmidt-number effects on the flow past a sphere moving vertically in a stratified diffusive fluid, Phys. Fluids **21**, 026602 (2009).
[12] A. Doostmohammadi, S. Dabiri, and A. M. Ardekani, A numerical study of the dynamics of a particle settling at moderate Reynolds numbers in a linearly stratified fluid, J. Fluid Mech. **750**, 5 (2014).
[13] A. Doostmohammadi and A. M. Ardekani, Suspension of solid particles in a density stratified fluid, Phys. Fluids **27**, 023302 (2015).
[14] H. Hanazaki, K. Kashimoto, and T. Okamura, Jets generated by a sphere moving vertically in a stratified fluid, J. Fluid Mech. **638**, 173 (2009).
[15] K. Y. Yick, C. R. Torres, T. Peacock, and R. Stocker, Enhanced drag of a sphere settling in a stratified fluid at small Reynolds numbers, J. Fluid Mech. **632**, 49 (2009).
[16] J. Zhang, M. J. Mercier, and J. Magnaudet, Core mechanisms of drag enhancement on bodies settling in a stratified fluid, J. Fluid Mech. **875**, 622 (2019).
[17] Y. Zvirin and R. S. Chadwick, Settling of an axially symmetric body in a viscous stratified fluid, Int. J. Multiphase Flow **1**, 743 (1975).
[18] F. Candelier, R. Mehaddi, and O. Vauquelin, The history force on a small particle in a linearly stratified fluid, J. Fluid Mech. **749**, 184 (2014).
[19] R. Mehaddi, F. Candelier, and B. Mehlig, Inertial drag on a sphere settling in a stratified fluid, J. Fluid Mech. **855**, 1074 (2018).
[20] I. Proudman and J. R. A. Pearson, Expansions at small Reynolds numbers for the flow past a sphere and a circular cylinder, J. Fluid Mech. **2**, 237 (1957).

[21] F. Blanchette and A. M. Shapiro, Drops settling in sharp stratification with and without Marangoni effects, Phys. Fluids **24**, 042104 (2012).
[22] D. W. Martin and F. Blanchette, Simulations of surfactant-laden drops rising in a density-stratified medium, Phys. Rev. Fluids **2**, 023602 (2017).
[23] M. Bayareh, A. Doostmohammadi, S. Dabiri, and A. M. Ardekani, On the rising motion of a drop in stratified fluids, Phys. Fluids **25**, 103302 (2013).
[24] M. Bayareh, S. Dabiri, and A.M. Ardekani, Interaction between two drops ascending in a linearly stratified fluid, Eur. J. Mech. B/Fluids **60**, 127 (2016).
[25] S. Dabiri, A. Doostmohammadi, M. Bayareh, and A.M. Ardekani, Rising motion of a swarm of drops in a linearly stratified fluid, Int. J. Multiphase Flow **69**, 8 (2015).
[26] C. Darwin, Note on hydrodynamics, Math. Proc. Cambridge Philos. Soc. **49**, 342 (1953).
[27] I. Eames, D. Gobby, and S. B. Dalziel, Fluid displacement by Stokes flow past a spherical droplet, J. Fluid Mech. **485**, 67 (2003).
[28] N. G. Chisholm and A. S. Khair, Drift volume in viscous flows, Phys. Rev. Fluids **2**, 064101 (2017).
[29] K. Katija and J. O. Dabiri, A viscosity-enhanced mechanism for biogenic ocean mixing, Nature (London) **460**, 624 (2009).
[30] K. Katija, Biogenic inputs to ocean mixing, J. Exp. Biol. **215**, 1040 (2012).
[31] S. Wang and A. M. Ardekani, Biogenic mixing induced by intermediate Reynolds number swimming in stratified fluids, Sci. Rep. **5**, 17448 (2015).
[32] R. Dandekar, V. A. Shaik, and A. M. Ardekani, Swimming sheet in a density stratified fluid, J. Fluid Mech. **874**, 210 (2019).
[33] A. M. Leshansky and L. M. Pismen, Do small swimmers mix the ocean? Phys. Rev. E **82**, 025301(R) (2010).
[34] G. Subramanian, Viscosity-enhanced bio-mixing of the oceans, Curr. Sci. **98**, 1103 (2010).
[35] A. M. Ardekani and R. Stocker, Stratlets: Low Reynolds Number Point-Force Solutions in a Stratified Fluid, Phys. Rev. Lett. **105**, 084502 (2010).
[36] E. Guazzelli, J. F. Morris, and S. Pic, *A Physical Introduction to Suspension Dynamics* (Cambridge University Press, Cambridge, 2011).
[37] T. D. Taylor and A. Acrivos, On the deformation and drag of a falling viscous drop at low Reynolds number, J. Fluid Mech. **18**, 466 (1964).
[38] L. G. Leal, *Advanced Transport Phenomena* (Cambridge University Press, Cambridge, 2007).
[39] S. Childress, The slow motion of a sphere in a rotating, viscous fluid, J. Fluid Mech. **20**, 305 (1964).
[40] P. G. Saffman, The lift on a small sphere in a slow shear flow, J. Fluid Mech. **22**, 385 (1965).
[41] M. J. Lighthill, *Introduction to Fourier Analysis and Generalised Functions* (Cambridge University Press, Cambridge, 1958).
[42] F. Candelier, R. Mehaddi, and O. Vauquelin, Note on the method of matched-asymptotic expansions for determining the force acting on a particle, arXiv:1307.6314.
[43] D. Legendre and J. Magnaudet, A note on the lift force on a spherical bubble or drop in a low-Reynolds-number shear flow, Phys. Fluids **9**, 3572 (1997).
[44] A. H. Nayfeh, *Introduction to Perturbation Techniques* (Wiley, New York, 1993).
[45] D. G. Voelz, *Computational Fourier Optics: A MATLAB Tutorial* (SPIE Press, Bellingham, WA, 2011).
[46] H. Brenner and R. G. Cox, The resistance to a particle of arbitrary shape in translational motion at small Reynolds numbers, J. Fluid Mech. **17**, 561 (1963).
[47] R. Dandekar, V. A. Shaik, and A. M. Ardekani, Motion of an arbitrarily shaped particle in a density stratified fluid, J. Fluid Mech. (to be published).
[48] M. Kojima, E. J. Hinch, and A. Acrivos, The formation and expansion of a toroidal drop moving in a viscous fluid, Phys. Fluids **27**, 19 (1984).
[49] C. J. Koh and L. G. Leal, The stability of drop shapes for translation at zero Reynolds number through a quiescent fluid, Phys. Fluids A **1**, 1309 (1989).
[50] V. A. Shaik and A. M. Ardekani, Point force singularities outside a drop covered with an incompressible surfactant: Image systems and their applications, Phys. Rev. Fluids **2**, 113606 (2017).

[51] N. Desai and A. M. Ardekani, Combined influence of hydrodynamics and chemotaxis in the distribution of microorganisms around spherical nutrient sources, Phys. Rev. E **98**, 012419 (2018).

[52] N. Desai, V. A. Shaik, and A. M. Ardekani, Hydrodynamics-mediated trapping of micro-swimmers near drops, Soft Matter **14**, 264 (2018).

[53] N. Desai, V. A. Shaik, and A. M. Ardekani, Hydrodynamic interaction enhances colonization of sinking nutrient sources by motile microorganisms, Front. Microbiol. **10**, 289 (2019).